



HAL
open science

Predicting pathogen-specific CD8 T cell immune responses from a modeling approach

Fabien Crauste, Emmanuelle Terry, Isabelle Le Mercier, Julien Mafille, Sophia Djebali, Thibault Andrieu, Blandine C. Mercier, Christophe Arpin, Jacqueline Marvel, Olivier Gandrillon, et al.

► To cite this version:

Fabien Crauste, Emmanuelle Terry, Isabelle Le Mercier, Julien Mafille, Sophia Djebali, et al.. Predicting pathogen-specific CD8 T cell immune responses from a modeling approach. *Journal of Theoretical Biology*, 2015, 374, pp.66-82. 10.1016/j.jtbi.2015.03.033 . hal-00717406v1

HAL Id: hal-00717406

<https://hal.science/hal-00717406v1>

Submitted on 12 Jul 2012 (v1), last revised 11 Dec 2015 (v2)

HAL is a multi-disciplinary open access archive for the deposit and dissemination of scientific research documents, whether they are published or not. The documents may come from teaching and research institutions in France or abroad, or from public or private research centers.

L'archive ouverte pluridisciplinaire **HAL**, est destinée au dépôt et à la diffusion de documents scientifiques de niveau recherche, publiés ou non, émanant des établissements d'enseignement et de recherche français ou étrangers, des laboratoires publics ou privés.

ESTIMATING RELEVANT PARAMETERS OF THE CD8 IMMUNE RESPONSE FROM A SYSTEMS BIOLOGY APPROACH

Emmanuelle Terry^{1,3}, Isabelle Le Mercier², Julien Mafille², Sophia Djebali²,
Thibault Andrieu², Blandine Mercier², Christophe Arpin², Fabien Crauste¹,
Jacqueline Marvel², Olivier Gandrillon^{3,4}

¹ Université de Lyon, Université Lyon 1, CNRS UMR 5208, Institut Camille Jordan,
43 blvd du 11 novembre 1918, F-69622 Villeurbanne-Cedex, France; INRIA Team Dracula,
INRIA Center Grenoble Rhône-Alpes

E-mail: terry@math.univ-lyon1.fr, crauste@math.univ-lyon1.fr

² INSERM, U851, 21 Avenue Tony Garnier, Lyon, F-69007 France; Université Lyon 1,
UMS3444/US8, France; Université de Lyon, France

E-mail: isabelle.lemercier@Dartmouth.edu, julien.mafille@inserm.fr, sophia.djebali@inserm.fr,
thibault.andrieu@inserm.fr, blandine.mercier@umassmed.edu, christophe.arpin@inserm.fr,
jacqueline.marvel@inserm.fr

³ Université de Lyon, Université Lyon 1, CNRS UMR 5534, Centre de Génétique et de
Physiologie Moléculaire et Cellulaire, F-69622 Villeurbanne-Cedex, France; INRIA Team
Dracula, INRIA Center Grenoble Rhône-Alpes

E-mail: olivier.gandrillon@univ-lyon1.fr

⁴ Corresponding author

Abstract

The primary immune response mediated by CD8 T cells constitutes a major mechanism to fight an infection by intra-cellular pathogens. This response begins with an expansion phase through a fast increase of CD8 T cell count. Then most of the population dies by apoptosis in a contraction phase, followed by the generation of memory cells. These latter are specific of the antigen and will better control the pathogen in a subsequent infection.

We generated experimental data, consisting in CD8 T cell numbers time evolution during the immune response to three different live intra-cellular pathogens, two viruses (influenza and vaccinia), and one bacteria (*Listeria monocytogenes*). These pathogens all harbour the same antigen, but differ in their interaction with the host, like the infection route. We are interested in characterizing how such differences translate into differences in the CD8 immune response.

We developed a mathematical model describing the evolution of CD8 T cell count and pathogen amount during the immune response. This model includes feedback controls that regulate the response, and is able to reproduce the characteristic dynamics

of the response. We have confronted this model to the three data series, and made an exhaustive estimation of the model parameters. We aim at determining not the best parameter which provides a good fit, but a set of parameter values which are suitable for a given parameter. This allows us to be more confident in evaluating the validity of the model and the influence of the parameters on the model. First we discuss how the suitable parameter values are different or not according to the fitted data series, and so according to the nature of the pathogen or the characteristics of the infection it generates. Then we refine the parameter values by discussing supplementary constraints on dynamics of memory cell subpopulation in the model. Finally we discuss how parameter values could be further validated, in particular with supplementary experimental investigations.

1 Introduction

The adaptative immune response constitutes one of the major mechanisms to fight infection by a pathogen. It involves a wealth of different cell types including B cells, CD4 and CD8 T lymphocytes and antigen presenting cells such as dendritic cells. Here, we focus on the cytolytic response mediated by CD8 T cells. These cells play an essential role in controlling infections by intra-cellular pathogens such as influenza viruses (Flu) (Ennis et al 1994; Wong and Pamer 2003; Kedzierska et al 2006), vaccinia virus (VV) (Snyder et al 2004; Jing et al 2005) or the bacteria *Listeria monocytogenes* (*Lm*) (Busch and Pamer 1999). We are interested in the characteristic dynamical behavior of the CD8 T lymphocytes responding to an infection by an intra-cellular pathogen (Murali-Krishna et al 1998). After pathogen encounter, these lymphocytes are activated and leave the naive state to enter an expansion phase associated with strong proliferation and differentiation into effector cells. CD8 effectors display cytotoxic capacities that allow them to kill infected cells and clear the pathogen. After the peak of proliferation concluding the expansion phase, most of the population dies by apoptosis, in a contraction phase. Effector cells can differentiate into memory cells, a crucial subpopulation able to respond more efficiently and to better control the pathogen in the case of a subsequent infection.

Different models based upon systems of ordinary differential equations were proposed to model the details of these kinetics of cell dynamics (De Boer et al 2001; Rouzine et al 2005; Kim et al 2007). In particular, Antia et al (2003, 2005) proposed a model with an age structure for the effector cell equation. They considered a limit age τ^* , such as when effector cells did not die before reaching this age $\tau = \tau^*$, then they differentiated into memory cells. Inspired by this model, we have developed a model with ordinary and age-structured differential equations (Terry et al 2012). It describes a primary response to an acute infection when the pathogen has never been encountered before and does not lead to a chronic infection. Effector cells can differentiate into memory cells, according to their age, and the two populations can be generated in parallel. Nonlinearities in the model account for biological feedback controls, able to regulate cell dynamics. Simulations were performed to qualitatively reproduce the data found in the literature (Murali-Krishna

et al 1998) and the model was able to fit correctly the phases of a primary response to a lymphocytic choriomeningitis virus (LCMV) infection in mice. Those simulations were only performed to reproduce qualitatively a "typical" CD8 T cell immune response, without going any further into a *bona fide* parameter analysis to investigate which values were able to really reproduce relevant kinetics of the response. Furthermore, viral load and replication were not considered, whereas they represent key parameters during an infection (Jing et al 2007; Lee et al 2009). Hence, to obtain a more realistic and versatile model that can describe CD8 responses to different pathogens, this infectious process must be taken into account. In this work, we therefore introduce pathogen replication into the model.

We compare the model to experimental data that were specifically generated for this purpose. These data consist in CD8 T cell numbers, measured during the CD8 T cell immune response to three different live intra-cellular pathogens (two viruses: an H1N1 Flu and the Western Reserve (WR) strain of VV; and one bacteria *Lm*). The three pathogens have been modified by reverse genetics to express the NP68 epitope that is recognized by the F5 T cell receptor (TCR). Hence, we can use transgenic naive CD8 T cells expressing the F5 TCR to monitor the response induced by these 3 different pathogens (H1N1-NP, VV-NP and *Lm*-NP). Although, these pathogens all activate a robust CD8 response, they differ in their interaction with the host in terms of host cells targeted, replication mechanisms and activation of the innate immune response.

Vaccinia virus infection provides protection against variola virus, the causative agent of smallpox, and stands as the classic example of a successful vaccine that confers life long protection. Vaccinia virus, an orthopoxvirus, is a large virus with a double-stranded DNA genome that replicates in the cytoplasm. The WR strain of vaccinia that is used in this study is a vaccinal strain that was adapted to the mouse (Parker et al 1941).

Despite their importance, T lymphocyte mechanisms involved in a vaccinia infection were not thoroughly studied (Snyder et al 2004). However, smallpox vaccines could be improved, since the existing vaccines are based on live viruses and stay contraindicated for some people (Oseroff et al 2008; Rehm et al 2009; Lantto et al 2011). Moreover vaccinia virus could also be used as a platform for the design of vaccines directed against other viruses (Snyder et al 2004).

Listeria monocytogenes is a Gram-positive bacterium that causes disease mainly in immunocompromised humans. Humans are exposed to *Lm* by ingesting contaminated foods such as dairy products. The Bacteria invades epithelial cells where it replicates. In mice, most studies of infection with *Lm* focus on immune responses to systemic infection following intravenous inoculation (Pamer 2004). The highly virulent 10403s strain was used in this study.

Influenza viruses are the causative agent of acute respiratory diseases. Influenza is an Orthomyxoviridae with a negative single-stranded RNA segmented genome that replicates in the nucleus. The WSN mouse adapted H1N1 strain was used in this study. Even more than vaccinia, influenza proves to be a topical problem, with the H1N1 pandemic for

example.

Influenza dynamics have been modeled quite extensively (see Smith et al (2010) and Beauchemin et al (2011)). First, influenza infection at population scale was widely studied, to model the spread of the infection by transmission between infected hosts. This type of models, mainly based on networks, can be used for health decisions, to limit epidemic spread, or determine a vaccine strategy (Alexander and Kobes 2011; Jing et al 2007; Mercer et al 2011). Yet these models do not provide any information on the mechanisms of the infection in the host, or how an infected organism reacts against the virus. More recently, within-host models for influenza infection appeared in various papers (Bocharov and Romanyukha 1994; Beauchemin et al 2005; Baccam et al 2006; Beauchemin et al 2008; Saenz et al 2010), allowing to focus on cellular mechanisms, reacting against virus introduction. Beauchemin et al (2005) developed a cellular automaton describing spread of the virus between target cells, in which the virus was not explicitly considered. This model was used to study the impact of the initial distribution of infected cells, regeneration of dead cells and proliferation of immune cells (Beauchemin 2006). Continuous models have also been considered where target cell and infected cell dynamics are described by ordinary differential equations, and replication of the virus is also described (Bocharov and Romanyukha 1994; Baccam et al 2006; Beauchemin et al 2008; Saenz et al 2010). In these types of models, the virus is produced in the infected cells, and its proliferation is limited by the number of uninfected cells. Some models also consider an eclipse phase, with a supplementary compartment, which corresponds to infected cells which are not yet able to produce viruses (Baccam et al 2006; Saenz et al 2010). To go further in the description of the antiviral defence mechanisms, some papers do study the role of interferon (Bocharov and Romanyukha 1994) or of the innate response (Saenz et al 2010) or the impact of drug treatments (Beauchemin et al 2008).

Since the immune response by cytotoxic lymphocytes plays a key role in the evolution of an influenza virus infection (Ennis et al 1994), immune cells have been added to the previous models of uninfected/infected cells (Chang and Young 2007; Handel et al 2010; Miao et al 2010; Tridane and Kuang 2010). In most of these models, an equation was added to describe the immune response, and the T cells were just labelled as activated or cytotoxic, without any further detail. Other authors decided to deal with many cell types involved in the immune response, such as effector cells, antigen presenting cells, B cells and Th1 and Th2 lymphocytes (Bocharov and Romanyukha 1994; Hancioglu et al 2009). Yet none of these models describes the naive, effector and memory states of the CD8 T cell population, or the possible crossregulations and feedbacks between these differentiation stages. Lee et al (2009) distinguished naive and effector CD8 T cells, but at the cost of an hypersophistication of the model which incorporated CD4 T cells in different states (naive, effector, mature...), B cells, dendritic cells, and uninfected and infected cells. The recirculation of these cells between different organs where the immune response takes place was also modeled. It resulted in a 48 parameter-model, that could not be submitted to a systematic parameter sweep. A key question in modeling biological systems indeed lies

within the estimation of relevant parameters of the model. For influenza, many previously described works compared their model to data. To do this, the authors estimated part of their parameters and/or used parameters from previously published models or published experimental data (Bocharov and Romanyukha 1994; Baccam et al 2006; Hancioglu et al 2009; Lee et al 2009; Handel et al 2010; Miao et al 2010; Saenz et al 2010). Nevertheless, data used were very heterogeneous and parameter values which were chosen remain difficult to validate, in the absence of a systematic parameter sweep (Beauchemin and Handel 2011).

In the present work, we aim to describe the mechanisms of a CD8 T cell immune response dynamic against infection by an intra-cellular pathogen. We take into account naive, effector and memory differentiation states which were not described in the previous models with uninfected/infected cells (Chang and Young 2007; Handel et al 2010; Miao et al 2010; Tridane and Kuang 2010). We make an exhaustive estimation of the model parameters, by confronting the model with influenza, vaccinia and listeria experimental data. We aim at determining not the best parameter which provides a good fit, but a set of parameter values which are suitable for a given parameter, allowing us to be more confident in evaluating the validity of the model and the influence of the parameters on the model. Thus we can observe how suitable parameter values are different according to the fitted data series, or are the same for the three data series. Fitting to three different data series also allows to track the impact of the parameters in infection mechanisms and robustness of the model.

2 Materials and Methods

2.1 Experimental work

Experiments were performed to measure the CD8 T cell responses to the three pathogens in vivo. CD8 T lymphocyte numbers were measured by flow cytometry during the course of the immune response that was triggered by infection. All experimental procedures were approved by our local ethics committee and accreditations have been obtained from French governmental agencies.

F5 TCR transgenic T cells recognizing the NP68 epitope were transferred by retro-orbital injection in congenic C57Bl/6 mice. To normalize the experiments the same number of naive F5 CD8 T cells (2.10^5) were transferred in the three models of infection. The influenza H1N1 WSN strain, the vaccinia WR strain and the Listeria 10403s strain were all modified by reverse genetics to express the NP68 epitope. H1N1-NP was constructed and produced by Drs. O. Ferraris and M. Ottmann in Pr. B. Lina's laboratory (Jubin et al 2012). VV-NP was constructed and produced by Dr. D.Y.L. Teoh in Pr. Sir A.J. McMichael's laboratory (Cottalorda et al 2009). *Lm*-NP was constructed and produced by Dr. B. Mercier in Drs. N. Bonnefoy-Bérard and G. Lauvau's laboratories (unpublished data). In three distinct experiments, mice were inoculated intranasally with (2.10^5 TCID₅₀)

H1N1-NP or (2.10^5 PFU) VV-NP or intravenously with 3000 *Lm*-NP bacteria, the day after the transfer of naive F5 CD8 T cells. Intranasal inoculation of the influenza or the vaccinia viruses leads to a localized infection of the lung, while intravenous inoculation of *Listeria* leads to a systemic infection of the host. Mice were briefly anesthetized with 3% isofluorane in an oxygen chamber before being transferred or infected intravenously with *Lm*-NP or profoundly anesthetized with 70 mg/kg of Ketamin and 9 mg/kg of Xylazin before intranasal infection with viruses.

For each experiment a cohort of 20 mice was used, alternate groups of 5 mice were bled at regular intervals to quantify F5 CD8 T cell numbers. Mice blood was sampled, at days 0, 3, 4, 5, 6, 10, 12, 14, 18, 21, 28, 38 postinfection for experiment with H1N1-NP, at days 4, 6, 7, 8, 11, 13, 15, 19, 22, 28, 35, 47 for experiment with VV-NP, and at days 3, 5, 7, 10, 12, 17, 34 for experiment with *Lm*-NP. The time course was designed in order to capture the different phases of the response, i.e. the activation-induced expansion, contraction and memory phases.

The volume of blood samples was measured to calculate CD8 T cell numbers and a given number of fluorescent calibration beads was added to each samples. Cells were then stained with fluorescent antibodies against CD8, CD45 and CD45.1 to identify the transferred F5 CD8 T cells. Samples were then analyzed by flow cytometry to detect F5 CD8 T cells and fluorescent beads. These calibration beads were used to re-calculate the concentration of F5 CD8 T cells per mL of blood and total numbers of F5 CD8 T cells were calculated, considering 2mL of blood per mouse.

In the following, we present the detailed model, constituted by a system of ordinary differential equations, that we developed and compared to the data.

2.2 Model

Mice were infected by three live pathogens that can replicate within the host. Naive CD8 T cells when they encounter their cognate peptide differentiate into effector cells able to eliminate the pathogen, and a fraction of these cells will then differentiate into memory cells (see Figure 1). We consider a system based on ordinary differential equations, describing the evolution of CD8 T cell numbers (naive, effector and memory cells), and of the pathogen count. This system includes 4 feedback functions, as cell differentiation, proliferation and death are strongly controlled by feedback loops, depending on interactions between the different CD8 populations (naive, effector, memory cell populations) and with the pathogen. For example, pathogen induces differentiation of naive cells into effector cells, and promotes proliferation of effector cells.

We denote by $N(t)$ the naive cell number at time t . Naive cells die with a constant rate μ_N , positive, and differentiate in effector cells with a rate $\delta_{NE}P(t)$ which depends on the pathogen count denoted by $P(t)$ (Appay and Rowland-Jones 2004).

We denote by $E(t)$ the effector cell number at time t . Effector cells proliferate with a rate $\rho_E P(t)$ which depends on the pathogen count (Appay and Rowland-Jones 2004;

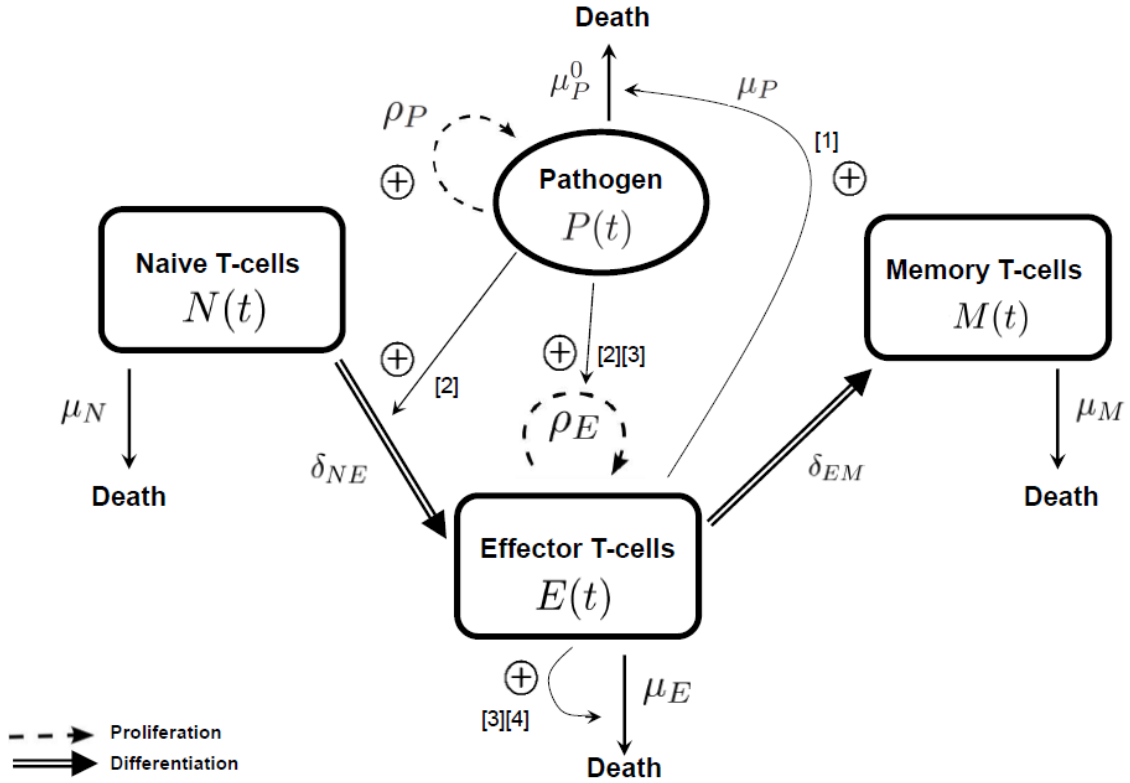


Figure 1: Schematic representation of the T CD8 immune response mechanisms after an infection by an intra-cellular pathogen, either influenza or vaccinia viruses, or listeria bacteria in our experiments. Biological justifications of this scheme are mentioned in Section 2.2, and referenced here by numbers: [1] Antia et al 2003, [2] Appay and Rowland-Jones 2004, [3] Kemp et al 2004, [4] Su et al 1993.

Kemp et al 2004; Kim et al 2007) and die with a rate $\mu_E E(t)$ which depends on their own number, due particularly to competition for limited resources such as cytokines, or fratricidal death (Su et al 1993; Kemp et al 2004). Effector cells can also differentiate in memory cells with a constant rate δ_{EM} .

We denote by $M(t)$ the memory cell number at time t . Memory cells die with a constant rate μ_M .

Finally, we denote by $P(t)$ the pathogen count at time t . We assume that pathogen proliferates with a rate $\rho_P P(t)$ which depends on its own count, and die with a rate $\mu_P E(t) + \mu_P^0$ in which $\mu_P E(t)$ depends on the effector cell number (Antia et al 2003), and $\mu_P^0 > 0$ is constant and corresponds to the natural death rate of pathogen.

Cell numbers $N(t)$, $E(t)$, $M(t)$ and the pathogen count $P(t)$ satisfy the following system of ordinary differential equations (Terry et al 2012), for $t > 0$:

$$\left\{ \begin{array}{l} \frac{dN}{dt}(t) = [-\mu_N - \delta_{NE}P(t)]N(t), \quad N(0) = N_0, \\ \frac{dE}{dt}(t) = \delta_{NE}P(t)N(t) + [\rho_E P(t) - \mu_E E(t) - \delta_{EM}]E(t), \quad E(0) = E_0, \\ \frac{dM}{dt}(t) = -\mu_M M(t) + \delta_{EM}E(t), \quad M(0) = M_0, \\ \frac{dP}{dt}(t) = [\rho_P P(t) - (\mu_P E(t) + \mu_P^0)]P(t), \quad P(0) = P_0. \end{array} \right. \quad (1)$$

We do not consider any production of naive cells from hematopoietic stem cells, as naive cells used in the experiments are exogenous and do not self renew in mice (see Section 2.1).

Finally, without dealing with initial conditions N_0 , E_0 , M_0 and P_0 , the model contains 9 constant parameters $\mu_N, \delta_{NE}, \rho_E, \mu_E, \delta_{EM}, \mu_M, \rho_P, \mu_P, \mu_P^0$. The goal is to determine which parameter values are able to fit the data, and how T-cell subpopulations, which can be simulated by the model, evolve with these parameters.

The values of N_0 , E_0 , M_0 are known from experimental data: a given number N_0 of purified naive CD8 T cells is injected at time $t = 0$ in mice, and in the absence of pathogen there are no effector or memory cells, so $E_0 = 0$ and $M_0 = 0$. However, the value of P_0 is not known, since in experimental data, dynamics of pathogen counts remain unknown. Hence, we should count P_0 as an other parameter to be determined, and the model would exhibit 10 free parameters. To avoid this supplementary difficulty, we re-scale the system (1) as follows.

Define $p(t) = P(t)/P_0$ where $P_0 > 0$. Then, $p(t)$ satisfies:

$$\frac{dp}{dt}(t) = [\rho_P P_0 p(t) - (\mu_P E(t) + \mu_P^0)]p(t), \quad \text{with } p(0) = 1.$$

With the same re-scaling, the equations for N and E in (1) become:

$$\frac{dN}{dt}(t) = [-\mu_N - \delta_{NE}P_0 p(t)]N(t),$$

$$\frac{dE}{dt}(t) = \delta_{NE}P_0 p(t)N(t) + [\rho_E P_0 p(t) - \mu_E E(t) - \delta_{EM}]E(t),$$

and the equation for M does not change. Finally, the re-scaled system (1) is:

$$\left\{ \begin{array}{l} \frac{dN}{dt}(t) = [-\mu_N - \bar{\delta}_{NE}P(t)]N(t), \quad N(0) = N_0, \\ \frac{dE}{dt}(t) = \bar{\delta}_{NE}P(t)N(t) + [\bar{\rho}_E P(t) - \mu_E E(t) - \delta_{EM}]E(t), \quad E(0) = E_0, \\ \frac{dM}{dt}(t) = -\mu_M M(t) + \delta_{EM}E(t), \quad M(0) = M_0, \\ \frac{dP}{dt}(t) = [\bar{\rho}_P P(t) - (\mu_P E(t) + \mu_P^0)]P(t), \quad P(0) = 1, \end{array} \right. \quad (2)$$

where, for the sake of simplicity, we still denote the pathogen count by $P(t)$, and $\bar{\delta}_{NE} = \delta_{NE}P_0$, $\bar{\rho}_E = \rho_E P_0$, $\bar{\rho}_P = \rho_P P_0$. Consequently, the parameters $\bar{\delta}_{NE}, \bar{\rho}_E, \bar{\rho}_P$ have not the same meaning than in the system (1). However, it does not change the method to estimate all the parameters, described in Section 3.3, so it does not add any difficulty, and for the sake of simplicity, we will keep the notations $\delta_{NE}, \rho_E, \rho_P$ in the following. A detailed analysis of the system (2) (existence of steady states and their linear stability) is presented in Supplementary Material. In the following, we describe the method we used for simulating the model in order to fit it to the data, and to make an exhaustive estimation of the model parameters.

2.3 Simulations

We performed an exhaustive exploration of the parameter value space, by computing solutions of system (2), using 5 distinct values for each of the 9 parameters. It resulted in 5^9 combinations of parameters, that is to say 1,953,125 simulations. Tested parameter values are presented in Section 3.2. Simulations were performed using facilities of the Calculus Center of the National Institute of Nuclear Physics and Particle Physics (IN2P3). The 250 cores of IN2P3 were used to distribute the large number of needed simulations, within 7,812 simulations per core for the 249 first cores, and 7,937 simulations for the last core. For each simulation, the error ε between the experimental data points x_i measured at time t_i and the corresponding simulated point $x(t_i)$ was determined using a least-square method, with the formula

$$\varepsilon = \sqrt{\sum_i (\log x_i - \log x(t_i))^2}.$$

This method was chosen for its easy implementation, and for its quickness to compute the error. As the model is based on the description of the dynamics of T-cell subpopulations (naive, effector and memory cells), whereas experimental data correspond to a total T CD8 population count, the value of each simulated point $x(t)$ is equal to $N(t)+E(t)+M(t)$. All these computed errors were ranked in increasing order. Hence, the smallest errors correspond to the best fits and we can focus on the corresponding parameter sets (see Figure

2 for an illustration of the method). It is noted that it is not relevant to compare error values between experiments (influenza, vaccinia and listeria), as only rank of errors is relevant. Many parameter sets lead to an unbounded solution of the system (2). They correspond to computed simulations which do not provide any correct immune response, with respect to experimental data, since proliferation of the pathogen is not limited by CD8 T cells. Such simulations cannot fit experimental data. For these parameter sets, the value of -1 was assigned to the corresponding error, and these values were deleted before treating the results. Such combinations of values represent around 28% of the total number of the tested parameter sets. In the following, we consider the simulations which lead to a bounded solution that is with an error value not equal to -1 .

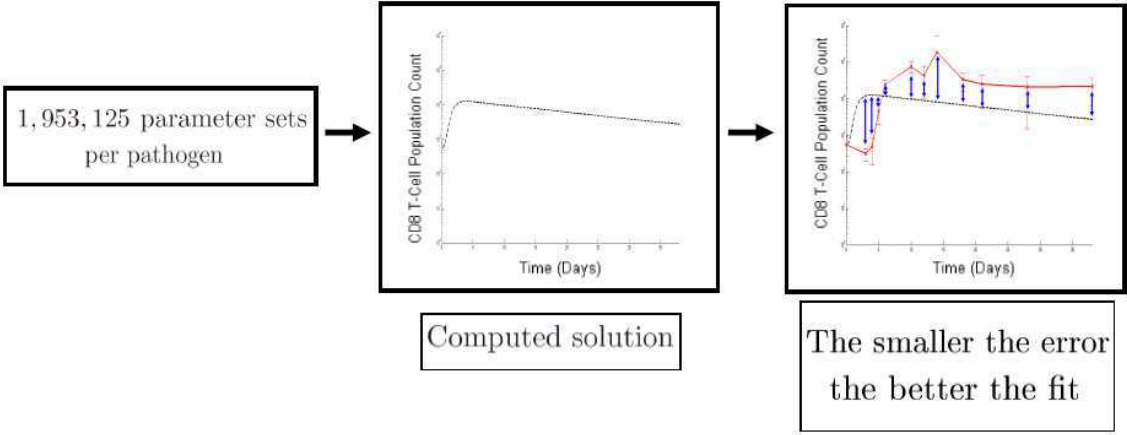


Figure 2: The different steps of the analysis that were followed to determine the parameter sets able to fit the model (black curve) on the data (red linked points).

Distribution of error values is computed (see Figure 6 in Supplementary Material). Among the error values in the interval $[10, 20]$, which represent around 60% of all considered computed errors, many errors correspond to parameter sets producing flat responses (see Figure 7 in Supplementary Material for an example). These simulations are unable to describe cellular expansion and contraction phases, observed in experimental data. This justifies considering $\varepsilon = 10$ as a threshold value: above this value, fits will be described as "bad fits". For each data series (influenza, vaccinia and listeria), around 20% of error values are inferior or equal to 10. However, keeping all the parameter sets with an error inferior or equal to 10 is still too large. For example, if we restrict the study to the 14,003 smallest errors (1% of the smallest errors), the 14,003th error is equal to 3.8, yet the corresponding parameter set leads to a fit which does not capture the phases of the response and thus is not qualitatively correct (see Figure 8 in Supplementary Material). Hence, keeping only parameters corresponding to the 1% of the lowest errors for the analysis is still too large. Finally, the number of error values corresponding to correct fits may be

restricted to 0.01% of best parameter sets, which correspond to an error less or equal to 3. We hereafter present the results of the experimental work and of the simulations performed on the model, and in particular, we discuss the results obtained with parameter sets able to fit the data.

3 Results

3.1 Data

Five measurements of F5 CD8 T cell counts were performed on different time points after infection with influenza, vaccinia or listeria (see Section 2.1). Experimental responses are presented on Figure 3 where each point corresponds to the mean of the five experimental points, with its associated standard deviation. The initial value of naive cells that grafted in the host was experimentally measured in the influenza experiment. As the same number of F5 CD8 T cells was used for all experiments, the same initial value is considered for vaccinia and listeria experiments. For each data series, a typical qualitative behaviour of a CD8 T cell immune response can be observed, with a strong expansion from days 3 – 4 postinfection, a peak of response which occurs on day 7 postinfection for listeria experiment, and later, around day 10 for influenza and vaccinia experiments. The peak is followed by a contraction phase until day 20 postinfection, and a stabilization of lymphocyte population counts above the initial naive value. Influenza and vaccinia data lead to similar responses, whereas the CD8 response against listeria seems to be different, with an earlier and stronger proliferation of lymphocytes. Indeed, the peak for listeria response reaches $6 \cdot 10^5$ cells while the peak does not overtake 10^5 cells for influenza and vaccinia data. This suggests that the class of pathogen and/or the route of inoculation induces different profiles of CD8 T cell responses.

3.2 Tested parameter sets of the model

The CD8 T cell immune responses against the three pathogens were modeled as presented in Figure 1. This model is characterized by 9 parameters (see Section 2.2), and no a priori knowledge of parameter values was available to help us to determine which values should be preferentially tested. In the following, we focus on the parameter values, which are constant, but it must be kept in mind that some parameters are associated to non-constant biological rates. This point is detailed in Table 1.

We have explored parameter sets to fit the model to the data, first to influenza data, followed by vaccinia and listeria data. Our method was to test a maximum of parameter sets to be as exhaustive as possible. Tested parameter values are chosen under the constraint of staying reasonable from a modeling point of view: for example, if parameter ρ_P is taken equal to 100, it appears that in most of the simulations, the pathogen count in the model increases infinitely. Hence such parameter value seems too large to ensure a realistic immune response. Tested parameter sets are also chosen to take into account

as much as possible known biological metrics (see legend of Table 2), even if some values look extreme: the goal of this exhaustive parameter estimation remains to investigate as large a range of parameter sets as possible, and this idea of systematic parameter sweep leads to keep large intervals of values. Ranges for each parameter are determined under these conditions and five values distributed in the interval are tested (see Table 2). These five values for each parameter have been determined after running numerous preliminary trials (data not shown).

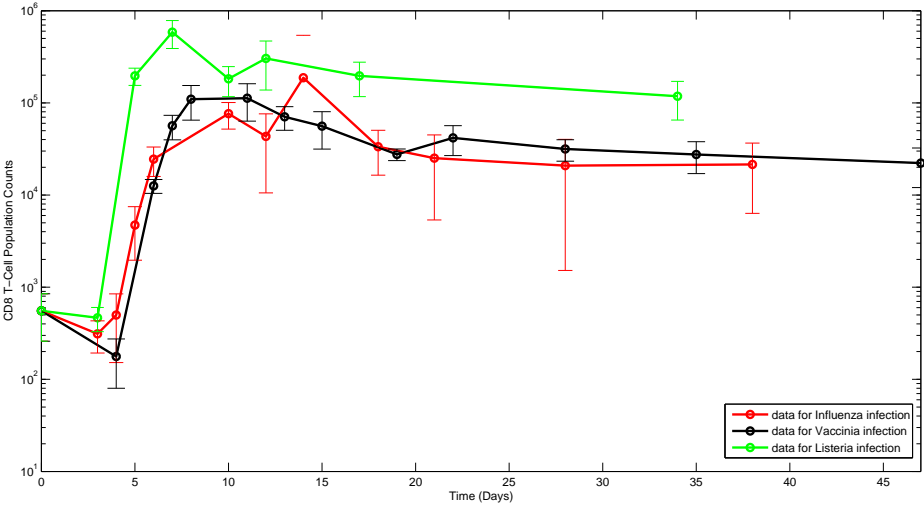


Figure 3: Experimental data: F5 CD8 T cell counts for influenza (red) and vaccinia (black) virus infections and listeria bacterium (green) infection. Each data point corresponds to the mean and standard deviation of CD8 T cells numbers from 5 individual mice.

Table 1: Link between the parameters considered and the biological rates of the model. Graphic illustration is shown for the parameter values corresponding to the best fit of the model using the influenza data (see Section 3.3 with Table 4).

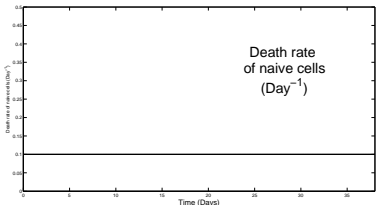
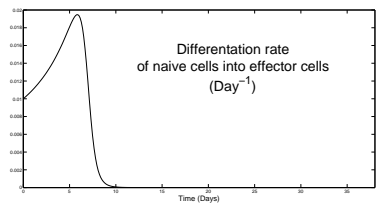
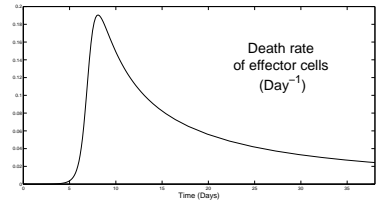
Link between a parameter and the corresponding biological rate	Parameters in day^{-1} or in $cell^{-1} day^{-1}$	Corresponding biological rates in day^{-1}	Evolution of the biological rate (in day^{-1}) during the response
Parameters, expressed in day^{-1} , which model directly <i>constant</i> biological rates	$\mu_N, \delta_{EM}, \mu_M, \mu_P^0$	$\mu_N, \delta_{EM}, \mu_M, \mu_P^0$	μ_N 
Parameters, expressed in day^{-1} , which are associated to <i>non constant</i> biological rates	$\delta_{NE}, \rho_E, \rho_P$	$\delta_{NE}P(t), \rho_E P(t), \rho_P P(t)$	$\delta_{NE}P(t)$ 
Parameters, expressed in $cell^{-1} day^{-1}$, which are associated to <i>non constant</i> biological rates	μ_E, μ_P	$\mu_E E(t), \mu_P E(t)$	$\mu_E E(t)$ 

Table 2: Parameter values tested in simulations of the model described by system (2). To have an idea of the biological meaning of these values, one can consider the following examples of parameter values associated to a death rate, a differentiation rate and a proliferation rate. When $\mu_N = 10^{-4} \text{ day}^{-1}$, it corresponds to the death of 0.01% of naive CD8 T cells per day, and when $\mu_N = 1 \text{ day}^{-1}$, it corresponds to the death of 63% of cells per day. When $\delta_{EM} = 10^{-3} \text{ day}^{-1}$, it corresponds to the differentiation of 0.1% of effector cells in memory cells per day, and when $\delta_{EM} = 10 \text{ day}^{-1}$, it corresponds to the differentiation of 100% of effector cells in memory cells per day. When $\rho_E = 10^{-1} \text{ day}^{-1}$, it corresponds to almost quiescent effector cells (1.5 division of an effector cell per ten days), and when $\rho_E = 10 \text{ day}^{-1}$, it corresponds to 14 divisions of an effector cell per day. Tested values are taken sufficiently large to ensure an exhaustive estimation of parameters, even if some values are certainly too extreme to correspond to real biological metrics. Parameters μ_E and μ_P ($\text{cell}^{-1} \text{ day}^{-1}$) do not directly correspond to cell rates, so their biological meaning is more difficult to define.

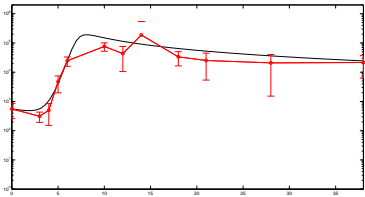
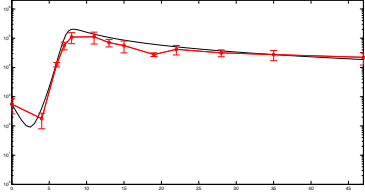
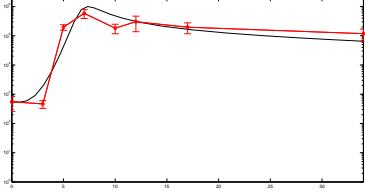
Biological rate	Parameter	Parameter unit	Tested values				
Death rate of naive cells	μ_N	Day^{-1}	10^{-4}	10^{-3}	10^{-2}	10^{-1}	1
Differentiation rate of naive cells in effector cells	δ_{NE}	Day^{-1}	10^{-2}	5.10^{-2}	10^{-1}	5.10^{-1}	1
Proliferation rate of effector cells	ρ_E	Day^{-1}	10^{-1}	5.10^{-1}	1	5	10
Death rate of effector cells	μ_E	$\text{Cell}^{-1} \text{ Day}^{-1}$	10^{-8}	5.10^{-8}	10^{-7}	5.10^{-7}	10^{-6}
Differentiation rate of effector cells in memory cells	δ_{EM}	Day^{-1}	10^{-3}	10^{-2}	10^{-1}	1	10
Death rate of memory cells	μ_M	Day^{-1}	5.10^{-2}	10^{-1}	5.10^{-1}	1	5
Death rate of pathogen dependent on effector cells	μ_P	$\text{Cell}^{-1} \text{ Day}^{-1}$	10^{-8}	10^{-7}	10^{-6}	10^{-5}	10^{-4}
Natural death rate of pathogen	μ_P^0	Day^{-1}	10^{-3}	10^{-2}	10^{-1}	1	10
Proliferation rate of pathogen	ρ_P	Day^{-1}	10^{-3}	10^{-2}	10^{-1}	1	10

3.3 Fits on the data

Combinations of the 5 values presented in the previous section for each of the 9 parameters were tested. The error between experimental data points and the corresponding simulated values was computed for each parameter set (see Section 2.3 for details).

The smallest error values obtained are equal to 2 for influenza experiments, 1.6 for vaccinia experiments, and 2.4 for listeria experiments. For these values, the corresponding simulations with the selected parameter sets are presented in Table 3. We obtained correct fits on total CD8 T lymphocyte population for the different data series, showing the expected phases of expansion and contraction with a correct quantitative behavior. For these simulations, a group of parameters, ρ_E , μ_E , δ_{EM} and ρ_P , presents exactly the same values for all three pathogens (see Table 3). It suggests these parameters reproduce the correct general behavior of the response observed in the three data series, as the three infections trigger a similar qualitative response, that is an expansion phase followed by a peak and a contraction phase. But what is also relevant consists in the differences in parameter values which appear between influenza/vaccinia infections on one hand and listeria infection on the other hand, since δ_{NE} , μ_M , μ_P and μ_P^0 have the same value for influenza and vaccinia simulations but a different value for listeria simulation. It suggests that this group of parameters distinguishes a response against a local infection by a virus such as influenza or vaccinia and a systematic response against a bacteria such as listeria.

Table 3: Best fits for the three experiments, and the corresponding parameter values of the model. Each graph displays the total T CD8 population count simulated (in black), and experimental data with standard deviation (red points) over the duration (in days) of each experiment. The value $\rho_E = 1 \text{ day}^{-1}$ corresponds to 0.8 division for an effector cell per day. The value $\delta_{EM} = 10^{-2} \text{ day}^{-1}$ corresponds to a differentiation of 1% of effector cells into memory cells per day. The value $\rho_P = 10^{-1} \text{ day}^{-1}$ corresponds to a pathogen that proliferates at an extremely low rate (1.5 division per ten days). The value $\mu_N = 10^{-1}$ (respectively 1) day^{-1} corresponds to a death of 10% (respectively 63%) of naive cells per day. The value $\delta_{NE} = 10^{-2}$ (respectively 10^{-1}) day^{-1} corresponds to a differentiation of 1% (respectively 10%) of naive cells into effector cells per day. The value $\mu_M = 5.10^{-2}$ (respectively 5) day^{-1} corresponds to a death of 5% (respectively 99%) of memory cells per day. The value $\mu_P^0 = 10^{-3}$ (respectively 10^{-2}) day^{-1} corresponds to a natural death of 0.1% (respectively 1%) of pathogen per day. Parameters μ_E and μ_P ($\text{cell}^{-1} \text{ day}^{-1}$) do not directly correspond to cell rates, so their biological meaning is more difficult to define.

Best fits for each experiment	Associated parameter values								
	ρ_E (Day^{-1})	μ_E ($\text{Cell}^{-1} \text{ Day}^{-1}$)	δ_{EM} (Day^{-1})	ρ_P (Day^{-1})	μ_N (Day^{-1})	δ_{NE} (Day^{-1})	μ_M (Day^{-1})	μ_P ($\text{Cell}^{-1} \text{ Day}^{-1}$)	μ_P^0 (Day^{-1})
Influenza experiment 	1	10^{-6}	10^{-2}	10^{-1}	10^{-1}	10^{-2}	5	10^{-5}	10^{-2}
Vaccinia experiment 	1	10^{-6}	10^{-2}	10^{-1}	1	10^{-2}	5	10^{-5}	10^{-2}
Listeria experiment 	1	10^{-6}	10^{-2}	10^{-1}	10^{-1}	10^{-1}	5.10^{-2}	10^{-6}	10^{-3}

3.4 Parameter range

We investigate the frequency of appearance of each parameter value, in the parameter sets corresponding to the 0.01% of the smallest classified errors. Indeed, if we consider 1% of the smallest errors, the simulation results for the three data series are not qualitatively correct for the worst cases (see Figure 8 in Supplementary Material for an example). Hence, we decided to restrict our study to the 0.01% of parameter sets with the smallest errors, that is to say approximately 140 parameter sets. It can be noted that in this group of 0.01% of best parameter sets, errors have values less than or equal to 3 and provide fits on the data that are very similar qualitatively and quantitatively. Differences between the 140 computed solutions appeared in the kinetics of the subpopulations, and not really in the total population kinetic, which is fitted.

In Section A.1 of Supplementary Material, conditions for existence and stability of steady states of the model are studied. For the 140 best parameter sets, a small number of fits (3 for influenza experiment, 30 for vaccinia experiment and none for listeria experiment) satisfies conditions (4), ensuring existence of the positive steady state. Nevertheless, it appears that the condition $\mu_E > \mu_P$ is never satisfied. Hence, stability of steady state with a positive number of effector cells and pathogen can never occur within this relevant parameter range. The only possible stable steady state is the one without effector cells and pathogen, which is coherent with the expected behaviour on a long time: we do not consider a chronic infection, and the pathogen should be eliminated, while effector cells are not maintained in the organism.

It appears that parameters ρ_E for the effector cell proliferation and μ_P for the pathogen death depending on effector cells are strongly constrained in the 0.01% best parameter sets for influenza, vaccinia and listeria infections (Table 4). In all parameter sets corresponding to the 0.01% of smallest errors, $\rho_E = 1 \text{ day}^{-1}$, for influenza and listeria infections. For vaccinia infection, in 65% of the 0.01% best parameter sets, $\rho_E = 1 \text{ day}^{-1}$, and in 35% of the 0.01% best parameter sets, $\rho_E = 5 \cdot 10^{-1} \text{ day}^{-1}$. For μ_P , the value $10^{-5} \text{ cell}^{-1} \text{ day}^{-1}$ is chosen at 89% for influenza infection, at 93% for vaccinia infection, and at 63% for listeria infection. The value $\mu_P = 10^{-6}$ is chosen at 11% for influenza infection, at 7% for vaccinia infection, and at 37% for listeria infection. These values are not on the bounds of the intervals of the tested parameter values, as the tested values were in intervals $[10^{-1}, 10]$ for ρ_E , and $[10^{-8}, 10^{-4}]$ for μ_P . This allows us to be confident on the fact that a suitable value could not be outside the selected interval.

Other frequently chosen parameter values are very close for influenza and vaccinia infections, whereas values chosen for listeria infection are very different. In the following, we name "tolerance" as the characteristic that more than 2 values are possible or not for a given parameter, in the 0.01% of best parameter sets we consider. Parameters δ_{NE} for differentiation rate of naive into effector cells, μ_P^0 for natural pathogen death rate and ρ_P for pathogen proliferation rate are chosen with a tolerance for different possible values in influenza and vaccinia experiments, whereas there is no tolerance in the values for listeria

experiment, since only one value of each of these parameters (values 10^{-1} , 10^{-3} and 10^{-1} day $^{-1}$ respectively) is chosen with listeria experiment. On the contrary, parameter μ_E for effector cell death presents a tolerant choice of four values for listeria experiment, whereas only one value, 10^{-6} cell $^{-1}$ day $^{-1}$, is selected for influenza and vaccinia experiments. Selected values of parameter μ_N for naive cell death are opposite between influenza and vaccinia experiments on one hand and listeria experiment on the other hand, since the value 1 day $^{-1}$ is preferentially chosen for influenza and vaccinia, and is the only one which does not appear as a possible value for listeria experiment. It suggests that these parameters allow to distinguish the CD8 T cell immune response against a virus infection such as influenza or vaccinia and against a bacteria infection such as listeria. It is noted that what is observed here is the context of the response since all these responses are directed against the same antigen. Parameters δ_{EM} , for differentiation of effector cells in memory cells, and μ_M , for memory cell death, do not present any preferentially chosen value or any distinction between pathogen experiments. But if we would consider the subpopulation kinetics, we will see in the following that we could obtain additional discriminations between values of parameters which were not preferentially chosen in a first time.

3.5 Refining parameter values

The fit is performed on the sum $N(t) + E(t) + M(t)$ of the three subpopulations of lymphocytes, nevertheless, the model described by system (2) simulates explicitly the three subpopulations and allows to follow their kinetics after the pathogen introduction (see Figure 4). Thus the model brings relevant information, by providing the subpopulation kinetics corresponding to a fit on the total population which correctly reproduces the experimental data. The behavior of these subpopulations can therefore be used for restricting the relevant parameter values.

In the three best fits of each experiment (influenza, vaccinia and listeria experiments), it appears that there is always more effector cells than memory cells, which are not generated in large quantities, and that effector cells are maintained on a long time (see Figure 9 in Supplementary Material for an example with the best fit on influenza infection data). An additional way to discriminate between parameter values could therefore be to track parameter sets leading to a case where the memory cell number is larger than the effector cell number after 50 days postinfection. Indeed, it is more realistic to have a strong generation of memory cells still present in the organism many days after infection, whereas effector cells disappear earlier than memory cells. In the 0.01% of best parameter sets we considered, 10 parameter sets for influenza experiment, 6 for vaccinia experiment and none for listeria experiment correspond to a fit presenting such a crossing between effector cell and memory cell population counts. Hence, it represents a very small number of the 140 best parameter sets considered. For listeria experiment, it could be possible to consider less good fits than in the 0.01% of best parameter sets. However, if fits with the expected crossing between effector cell and memory cell counts existed, it would come at the expense

a poorer quality of the fit on experimental data. For influenza and vaccinia experiments, studying the small number of fits with a crossing between effector cell and memory cell population counts brings supplementary conditions on parameter values. Indeed, this constraint of crossing leads, for example in influenza experiment, to an other best fit (see Figure 5) than the previous one presented in Table 3 (or Figure 4). The error value for this other fit is 2.2 which is very close to the smallest value 2. This new fit of the total lymphocyte population count is not significantly different from the previous one, as all the fits corresponding to the 0.01% of best parameter sets are similar. But the generation of memory cells is more relevant, as there are more memory cells than effector cells at day 38 postinfection (3.10^3 effector cells and 10^4 memory cells).

Furthermore, since the model allows us to follow these subpopulation kinetics on a time that extends much further than the experimentally measured points, one can see that memory cells are maintained longer than effector cells, during 150 days postinfection, which represents around 30 days more than effector cells (see Figure 10 in Supplementary Material). The main difference between these two best fits consists in the value of the parameter μ_M which characterizes memory cell death. This parameter is equal to 5 day^{-1} in the best fit without a crossing between effector cell and memory cell population counts. It represents a death of 99% of memory cells per day, and it is reasonable to assume that this value is really too high from a biological point of view. The lack of memory cell generation in the best fit of Figure 4 confirms this idea. On the contrary, the parameter μ_M is equal to 10^{-1} day^{-1} in the best fit presenting a crossing between effector cell and memory cell population counts. It represents a death of 9.5% of memory cells per day, which is more reasonable.

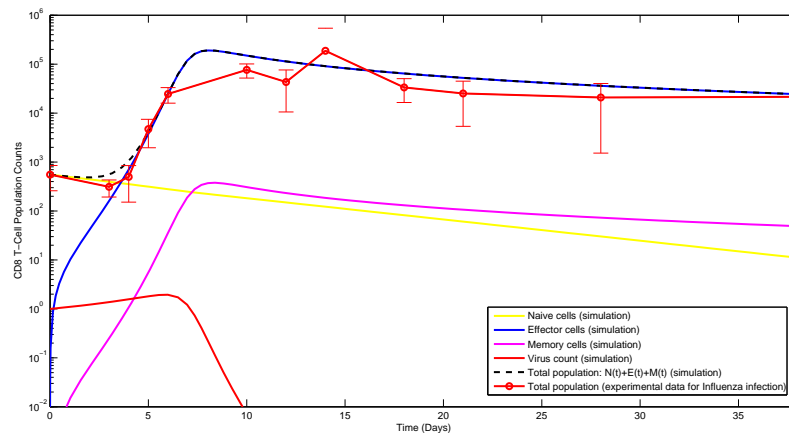


Figure 4: Best fit on experimental data for influenza infection, with the subpopulations of lymphocytes which appear in the model described by system (2). The yellow line corresponds to naive cell population kinetic, the blue line to effector cell population kinetic, the pink line to memory cell population kinetic, the dashed line to total population ($N(t) + E(t) + M(t)$) kinetic, the red line to pathogen count and the linked red points with error bar correspond to experimental data points.

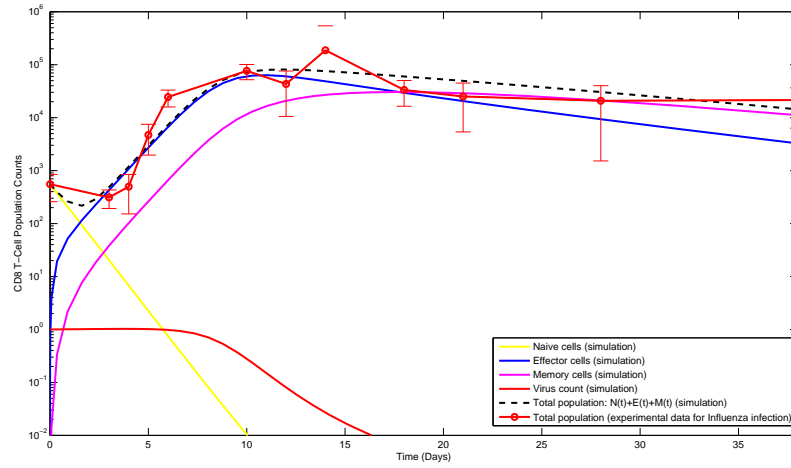


Figure 5: Best fit on experimental data for influenza infection, with the subpopulations of lymphocytes, with the constraint that a crossing between effector cell and memory cell population counts is expected, to ensure an efficient generation of memory cells. The yellow line corresponds to naive cell population kinetic, the blue line to effector cell population kinetic, the pink line to memory cell population kinetic, the dashed line to total population ($N(t) + E(t) + M(t)$) kinetic, the red line to pathogen count and the linked red points with error bar correspond to experimental data points.

4 Discussion

In many previous modeling works, where models were compared to data, only the best parameter set providing a good fit on the data was determined, but no systematic parameter sweep was performed (Lee et al 2009; Handel et al 2010). Yet this latter method allows being more confident if one wants to discuss validity of the model and influence of the parameters. In the present work, we considered a model of the CD8 T cell immune response, describing naive, effector and memory cell subpopulations kinetics, and where pathogen replication was considered. Specific experimental data were generated to confront our model to different dynamics of CD8 T cell immune responses, corresponding to three intra-cellular pathogens, two viruses, influenza and vaccinia, and one bacteria, listeria, all harbouring the same antigen (NP68).

To be able to perform this systematic investigation of parameters, we simulated the 5^9 combinations of parameters we aim at testing. The 5 tested values of each of the 9 parameters were chosen in order to obey two constraints: to keep a reasonable biological meaning while allowing to explore as much as possible a large interval. For each simulation, an error between experimental data and total CD8 T cell population count of the model was computed, using a least-squares method. We could have chosen another method to compute the error (genetic algorithm, bayesian approach...). But the least-squares method presents the two advantages of an easy implementation and fast computation of the error. These points are relevant in our approach, where we computed a very large amount of errors, and ran many trials to determine which parameter values are relevant to test. All these errors were ranked in increasing order. Hence, the smallest errors correspond to the best fits and we can focus on the corresponding parameter sets.

For each data series, influenza, vaccinia or listeria, good fits on the total lymphocyte population were performed. In each case, with restriction to the 0.01% of best parameter sets, corresponding fits are similarly able to reproduce the data. None of these sets satisfies the condition of stability of the steady state with a positive number of effector cells and pathogen (see Section A.1 of Supplementary Material). It ensures that the model reproduces a correct qualitative behavior, since effector cells and pathogen are not maintained in the long term, as expected from pathogens that do not lead to chronic infection. The frequency of each parameter was studied for the whole sets of parameters. Two parameters, ρ_E and μ_P , corresponding to the effector cell proliferation and the effector cell-dependent pathogen death rate, are determined for each infection with values $\rho_E = 1$ (0.8 division of an effector cell per day) and $\mu_P = 10^{-5}$ (not directly a rate with a biological meaning). A group of parameters is different between the response against viruses and the response against bacteria. These parameters are δ_{NE} for differentiation of naive cells in effector cells, μ_P^0 for natural pathogen death, ρ_P for pathogen proliferation, μ_E for effector cell death and μ_N for naive cell death. Three of those parameters characterize biological rates which depend on the pathogen nature or counts. This suggests that these parameters point to mechanisms of the immune response which change according to the

nature of the pathogen, or to the extent of pathogen spread, i.e. localized versus systemic infection. Further experimental investigations should be performed to confirm this idea. Cell rates could be experimentally tracked by using CFSE and viability dyes (Nordon et al 1999; Bernard et al 2003; De Boer and Perelson 2005; De Boer et al 2006) and the proliferation, differentiation and death rates of the model could be confronted to these new data. This would allow us to further validate these parameters. We could also induce a systemic infection with vaccinia through intravenous injection, in order to determine if the difference observed is due to the pathogen nature or to the extent of host infection.

Tracking the kinetics of the pathogen could also help to investigate differences between CD8 T cell immune responses against a virus or a bacteria. Confronting pathogen kinetic of the model to experimental pathogen kinetic could also help to validate model parameters. For influenza infection, experimental data available in the literature suggest that the viral dynamics mainly occur in the first 10 days postinfection (Wolk et al 2008; Desmet et al 2010; Garigliany et al 2010; Sun et al 2011). Wolk et al (2008) and Sun et al (2011) obtained experimental dynamics where the virus titer tends to increase until a peak (around day 3), then decrease. This behaviour is what we obtained for the pathogen kinetic in the model of response to influenza infection. What could be fitted more precisely is the time at which the peak of virus titer occurs, for example. But data in the literature are very heterogeneous and display few experimental points, only measured on a short period of time. Therefore we should perform experiments measuring pathogen count, including its initial count, at time 0. In this case, we would not have to re-scale the model by normalizing pathogen count by its initial value, as it would not remain unknown in the model. Then pathogen dynamic in the model could be confronted to the data, not only qualitatively, but also quantitatively.

An other point that could be further investigated is the fit of the subpopulations of naive, effector and memory cells described in the model. Indeed, the 0.01% of best parameter sets lead to similar fits on total CD8 T cell population, with close error values. Yet we can distinguish between these fits by looking at the subpopulation kinetics. In particular, a characteristic of these kinetics remains the crossing between effector cell and memory cell population counts. At the end of the response, a number of memory cells larger than the number of effector cells is expected, as memory cells are generated to fight against a second infection by the same pathogen, and effector cells just die by apoptosis during the resolution of the infection. But in a certain number of the 0.01% best fits, memory cell count always remains below the effector cell count. We could add a constraint in the study of the parameter sets, keeping only the sets corresponding to a fit where memory cell count becomes larger than effector cell count, during the response against each infection. The parameter sets determined in this case could be compared to the previous ones, and discriminate more precisely values corresponding to a real biological response. This observation points out the relevance on considering kinetics of the subpopulations of naive, effector and memory cells during a response. For example, the time during which memory cells are maintained could also be a relevant experimental

information to discriminate between the fits, not only with existence of a crossing between effector cell and memory cell counts, but also with the number of generated memory cells and the time during which these cells are maintained.

Fitting not only the total lymphocyte population count, but also the subpopulation kinetics should be a relevant method to obtain the maximum of information on model parameters. This study about subpopulation kinetics is currently under investigation: it is not a trivial experimental task to distinguish, at every time of the response, the different populations of naive, effector and memory cells. In particular, we still lack markers or combinations of markers that are uniquely expressed by these different CD8 differentiation states. Establishing such combinations would permit to generate data that could validate the model parameters.

A Supplementary Material

A.1 Steady states of the system (2) (see Section 2.2)

We study steady states of the system, and obtain conditions on parameters for existence and stability of these steady states. These conditions are relevant in the analysis of the parameter sets able to fit the model on the data, in Section 3.4.

A solution $(\bar{N}, \bar{E}, \bar{M}, \bar{P})$ of system (2) is a steady state if and only if $d\bar{N}/dt = d\bar{E}/dt = d\bar{M}/dt = d\bar{P}/dt = 0$, that is

$$\mu_N \bar{N} = -\delta_{NE} \bar{P} \bar{N}, \quad (3a)$$

$$\delta_{NE} \bar{P} \bar{N} = -[\rho_E \bar{P} - \mu_E \bar{E} - \delta_{EM}] \bar{E}, \quad (3b)$$

$$\mu_M \bar{M} = \delta_{EM} \bar{E}, \quad (3c)$$

$$\rho_P \bar{P}^2 = (\mu_P \bar{E} + \mu_P^0) \bar{P}. \quad (3d)$$

From equation (3a), we deduce that $\bar{N} = 0$. From equations (3b) and (3d), we obtain the following steady state values:

$$(\bar{E}, \bar{P}) = (0, 0), (\bar{E}, \bar{P}) = \left(0, \frac{\mu_P^0}{\rho_P}\right) \quad \text{and} \quad (\bar{E}, \bar{P}) = \left(\frac{\rho_P \delta_{EM} - \rho_E \mu_P^0}{\rho_E \mu_P - \mu_E \rho_P}, \frac{\mu_P \delta_{EM} - \mu_E \mu_P^0}{\rho_E \mu_P - \mu_E \rho_P}\right),$$

provided that

$$\frac{\rho_E}{\mu_E} > \frac{\rho_P}{\mu_P}, \quad \frac{\delta_{EM}}{\rho_E} > \frac{\mu_P^0}{\rho_P} \quad \text{and} \quad \frac{\delta_{EM}}{\mu_E} > \frac{\mu_P^0}{\mu_P}, \quad (4)$$

$$\text{or} \quad \frac{\rho_E}{\mu_E} < \frac{\rho_P}{\mu_P}, \quad \frac{\delta_{EM}}{\rho_E} < \frac{\mu_P^0}{\rho_P} \quad \text{and} \quad \frac{\delta_{EM}}{\mu_E} < \frac{\mu_P^0}{\mu_P}, \quad (5)$$

If one of the three conditions in (4) or (5) is not satisfied, then there exist two steady states $(\bar{E}, \bar{P}) = (0, 0)$ and $(\bar{E}, \bar{P}) = \left(0, \mu_P^0/\rho_P\right)$.

From the linearisation of system (2) around one of the steady states, we define the Jacobian matrix

$$A = \begin{pmatrix} -\mu_N - \delta_{NE} \bar{P} & 0 & 0 & 0 \\ \delta_{NE} \bar{P} & \rho_E \bar{P} - 2\mu_E \bar{E} - \delta_{EM} & 0 & \rho_E \bar{E} \\ 0 & \delta_{EM} & -\mu_M & 0 \\ 0 & -\mu_P \bar{P} & 0 & 2\rho_P \bar{P} - \mu_P \bar{E} - \mu_P^0 \end{pmatrix}.$$

The characteristic equation associated with the linearized system is then defined by

$$\det(\lambda I - A) = 0, \quad (6)$$

where I is the identity matrix in \mathbb{R}^3 . The steady states $(\bar{N}, \bar{E}, \bar{M}, \bar{P})$ of (2) are locally asymptotically stable if all roots of (6) have negative real parts, and are unstable when roots with positive real parts exist. After calculations, we obtain the following result:

1) The steady state $(\bar{N}, \bar{E}, \bar{M}, \bar{P}) = (0, 0, 0, 0)$ is locally asymptotically stable and the steady state $(\bar{N}, \bar{E}, \bar{M}, \bar{P}) = \left(0, 0, 0, \mu_P^0 / \rho_P\right)$ is unstable.

2) The steady state

$$(\bar{N}, \bar{E}, \bar{M}, \bar{P}) = \left(0, \frac{\rho_P \delta_{EM} - \rho_E \mu_P^0}{\rho_E \mu_P - \mu_E \rho_P}, \frac{\delta_{EM} (\rho_P \delta_{EM} - \rho_E \mu_P^0)}{\mu_M (\rho_E \mu_P - \mu_E \rho_P)}, \frac{\mu_P \delta_{EM} - \mu_E \mu_P^0}{\rho_E \mu_P - \mu_E \rho_P}\right), \quad (7)$$

which exists only when condition (4) or (5) holds true, is locally asymptotically stable only when (4) is satisfied and provided that the supplementary conditions $\frac{\rho_P \delta_{EM}}{\mu_E \mu_P^0} > \frac{\rho_E - \rho_P}{\mu_E - \mu_P}$ and $\mu_E > \mu_P$ hold true.

The result of existence and local asymptotic stability of the steady state $(\bar{N}, \bar{E}, \bar{M}, \bar{P}) = (0, 0, 0, 0)$ shows that solutions of (2), with no effector cells and an eliminated pathogen on a long time, which corresponds biologically to the resolution of the infection, can be expected, in particular if the non-trivial steady state defined in (7) is not locally asymptotically stable (for instance, if $\mu_E > \mu_P$).

A.2 Figures

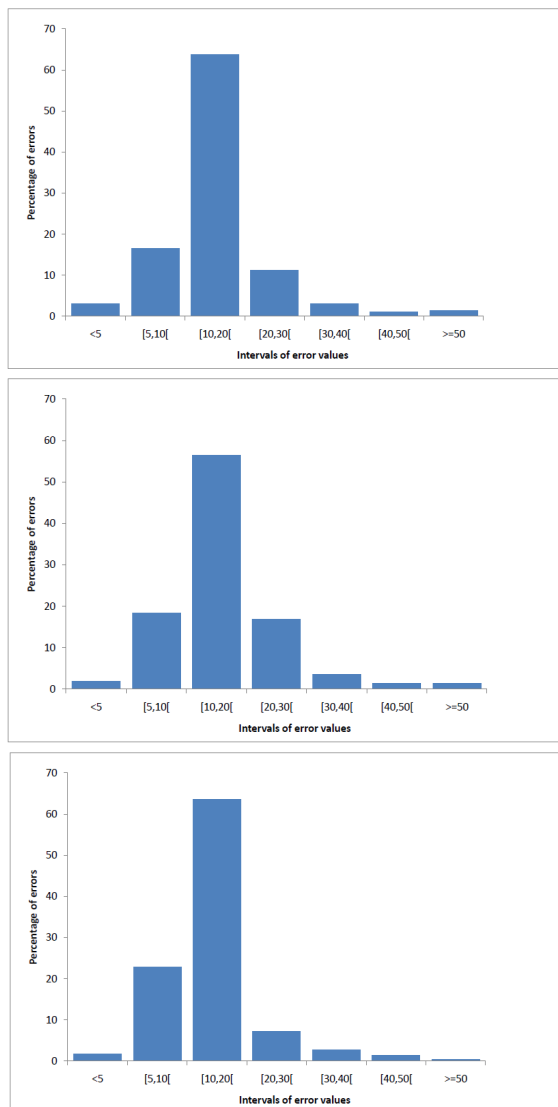


Figure 6: Distribution of error values. Top: influenza infection; Middle: vaccinia infection; Bottom: listeria infection. In each case, 0.01% of parameter sets (corresponding approximately to 140 sets) display an error value of less than 3.

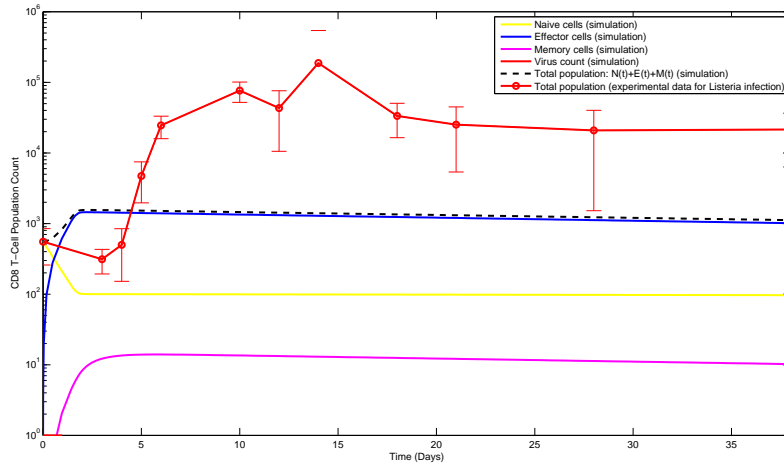


Figure 7: Example of a simulation resulting in a flat response, for fitting the model on influenza virus data. The yellow line corresponds to naive cell population kinetic, the blue line to effector cell population kinetic, the pink line to memory cell population kinetic, the dashed line to total population ($N(t) + E(t) + M(t)$) kinetic, the red line to pathogen count and the linked red points with error bar correspond to experimental data points.

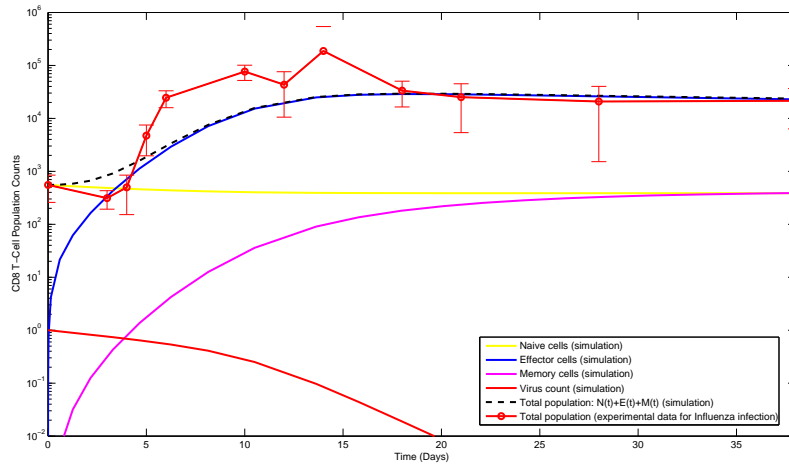


Figure 8: Example of a fit (the 14,003thrd in the ranking order of corresponding error value) qualitatively not correct, for fitting the model on influenza virus data. The yellow line corresponds to naive cell population kinetic, the blue line to effector cell population kinetic, the pink line to memory cell population kinetic, the dashed line to total population ($N(t) + E(t) + M(t)$) kinetic, the red line to pathogen count and the linked red points with error bar correspond to experimental data points.

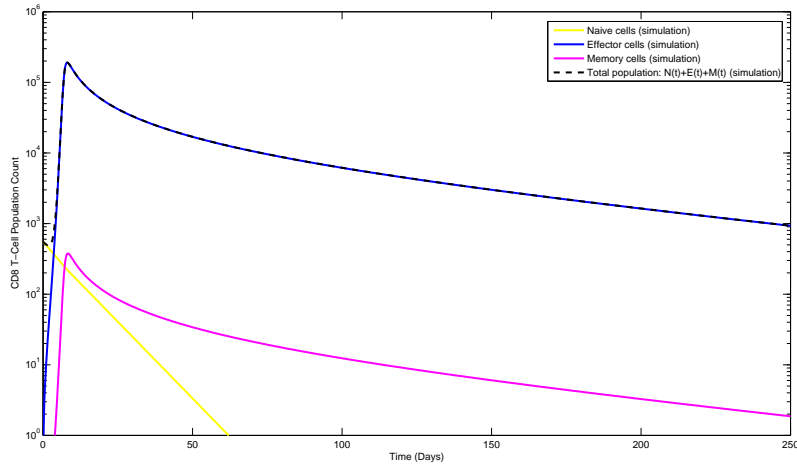


Figure 9: Best fit on experimental data for influenza infection, with the subpopulations of lymphocytes which appear in the model described by system (2), over 250 days. The yellow line corresponds to naive cell population kinetic, the blue line to effector cell population kinetic, the pink line to memory cell population kinetic and the dashed line to total population ($N(t) + E(t) + M(t)$) kinetic.

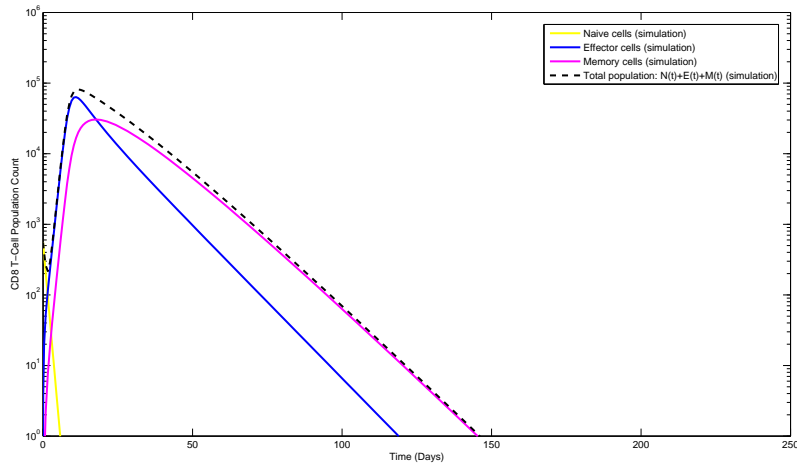


Figure 10: Best fit on experimental data for influenza infection, with the subpopulations of lymphocytes over 250 days, with the constraint that a crossing between effector cell and memory cell population counts is expected, to ensure an efficient generation of memory cells. The yellow line corresponds to naive cell population kinetic, the blue line to effector cell population kinetic, the pink line to memory cell population kinetic and the dashed line to total population ($N(t) + E(t) + M(t)$) kinetic.

B Acknowledgements

The authors thank IN2P3 and especially Pascal Calvat for their computing resources. We also thank Gaël Kaneko for his invaluable help in the use of the IN2P3 resources, Dr. Denise Yu-Lin Teoh and Pr. Sir Andrew J. McMichael for kindly providing the VV-NP vaccinia virus and Dr. Olivier Ferraris, Dr. Michelle Ottmann and Pr. Bruno Lina for the generation of the H1N1-NP influenza virus, and Dr. Grégoire Lauvau and Dr. Nathalie Bonnefoy-Bérard for the construction of the *Lm*-NP Listeria bacteria.

This work has been supported by the Finovi fondation, the Rhône-Alpes Complex System Institute (IXXI), the Fonds Européen de Développement Régional, and institutional grants from the Institut National de la Santé Et de la Recherche Médicale .

References

- Alexander M, Kobes R (2011) Effects of vaccination and population structure on influenza epidemic spread in the presence of two circulating strains. *BMC Public Health* 11(Suppl 1):S8
- Antia R, Bergstrom C, Pilyugin S, Kaech S, Ahmed R (2003) Models of CD8+ Responses: 1. What is the Antigen-independent Proliferation Program. *J Theor Biol* 221:585–598
- Appay V, Rowland-Jones S (2004) Lessons from the study of T-cell differentiation in persistent human virus infection. *Seminars in Immunol* 16:205–212
- Baccam P, Beauchemin C, Macken C, Hayden F, Perelson A (2006) Kinetics of Influenza A Virus Infection in Humans. *J Virol* 80:7590–7599
- Beauchemin C (2006) Probing the Effects of the Well-mixed Assumption on Viral Infection Dynamics. *J Theor Biol* 242(2):464–477
- Beauchemin C, Handel A (2011) A review of mathematical models of influenza A infections within a host or cell culture: lessons learned and challenges ahead. *BMC Public Health* 11(Suppl 1):S7
- Beauchemin C, Samuel J, Tuszynska J (2005) A simple cellular automaton model for influenza A viral infections. *J Theor Biol* 232:223–234
- Beauchemin C, McSharry J, Drusano G, Nguyen J, Went G, Ribeiro R, Perelson A (2008) Modeling amantadine treatment of influenza A virus in vitro. *J Theor Biol* 254:439–451
- Bernard S, Pujol-Menjouet L, Mackey M (2003) Analysis of cell kinetics using a cell division marker: mathematical modeling of experimental data. *Biophysical journal* 84:3414–3424
- Bocharov G, Romanyukha A (1994) Mathematical Model of Antiviral Immune Response III. Influenza A Virus Infection. *J Theor Biol* 167:323–360

- Busch D, Pamer E (1999) T lymphocyte dynamics during *Listeria monocytogenes* infection. *Immunology letters* 65:93–98
- Chang D, Young C (2007) Simple scaling laws for influenza A rise time, duration, and severity. *J Theor Biol* 246:621–635
- Cottalorda A, Mercier B, Mbitikon-Kobo F, Arpin C, Teoh D, McMichael A, Marvel J, Bonnefoy-Bérard N (2009) TLR2 engagement on memory CD8⁺ T cells improves their cytokine-mediated proliferation and IFN- γ secretion in the absence of Ag. *Eur J Immunol* 39:2673–2681
- De Boer R, Perelson A (2005) Estimating division and death rates from CFSE data. *Journal of computational and applied mathematics* 184:140–164
- De Boer R, Oprea M, Antia R, Murali-Krishna K, Ahmed R, Perelson A (2001) Recruitment Times, Proliferation, and Apoptosis Rates during the CD8 T-Cell Response to Lymphocytic Choriomeningitis Virus. *J Virol* pp 10,663–10,669
- De Boer R, Ganusov V, Milutinović D, Hodgkin P, Perelson A (2006) Estimating lymphocyte division and death rates from CFSE data. *Bulletin of mathematical biology* 68:1011–1031
- Desmet E, Hollenbaugh J, Sime P, Wright T, Topham D, Sant A, Takimoto T, Dewhurst S (2010) Mixed Lineage Kinase 3 deficiency delays viral clearance in the lung and is associated with diminished influenza-induced cytopathic effect in infected cells. *Virology* 400:224–232
- Ennis F, Yi-Hua Q, Riley D, Rook A, Schild G, Pratt R, Potter C (1994) HLA-Restricted Virus-Specific Cytotoxic T-Lymphocyte Responses to Live and Inactivated Influenza Vaccines. *J Theor Biol* 167:323–360
- Garigliany M, Habyarimana A, Lambrecht B, de Paar EV, Cornet A, Berg TVD, Desmecht D (2010) Influenza A strain-dependent pathogenesis in fatal H1N1 and H5N1 subtype infections of mice. *Emerg Infect Dis* 16:595–603
- Hancioglu B, Swigon D, Clermont G (2009) A dynamical model of human immune response to influenza A virus infection. *J Virol* 83:7151–7165
- Handel A, Longini I, J, Antia R (2010) Towards a quantitative understanding of the within-host dynamics of influenza A infections. *J R Soc Interface* 7:35–47
- Jing L, Chong T, McClurkan C, Huang J, Story B, Koelle D (2005) Diversity in the acute CD8 T cell response to vaccinia virus in humans. *J Immunol* 175:7550–7559
- Jing L, Chong T, Byrd B, McClurkan C, Huang J, Story B, Dunkley K, Aldaz-Carroll L, Eisenberg R, Cohen G, Kwok W, Sette A, Koelle D (2007) Dominance and diversity

- in the primary human CD4 T cell response to replication-competent vaccinia virus. *J Immunol* 178:6374–6386
- Jubin V, Ventre E, Leverrier Y, Djebali S, Mayol K, Tomkowiak M, Mafille J, Teixeira M, Teoh D, Lina B, Walzer T, Arpin C, Marvel J (2012) T inflammatory memory CD8 T cells participate to antiviral response and generate secondary memory cells with an advantage in XCL1 production. *Immunol Research* 52:284–293
- Kedzierska K, Gruta NL, Turner S, Doherty P (2006) Establishment and recall of CD8+ T-cell memory in a model of localized transient infection. *Immunol reviews* 211:133–145
- Kemp R, Powell T, Dwyer D, Dutton R (2004) Cutting Edge: Regulation of CD8⁺ T Cell Effector Population Size. *J Immunol* 179:2923–2927
- Kim P, Lee P, Levy D (2007) Modeling regulation mechanisms in the immune system. *J Theor Biol* 246:33–69
- Lantto J, Hansen MH, Rasmussen S, Steinaa L, Poulsen T, Duggan J, Dennis M, Naylor I, Easterbrook L, Bregenholt S, Haurum J, Jensen A (2011) Capturing the natural diversity of the human antibody response against vaccinia virus. *J Virol* 85:1820–1833
- Lee H, Topham D, Park S, Hollenbaugh J, Treanor J, Mosmann T, Jin X, Ward B, Miao H, Holden-Wiltse J, Perelson A, Zand M, Wu H (2009) Simulation and Prediction of the Adaptive Immune Response to Influenza A Virus Infection. *J Virol* 83:7151–7165
- Mercer G, Barry S, Kelly H (2011) Modelling the effect of seasonal influenza vaccination on the risk of pandemic influenza infection. *BMC Public Health* 11(Suppl 1):S11
- Miao H, Hollenbaugh J, Zand M, Holden-Wiltse J, Mosmann T, Perelson A, Wu H, Topham D (2010) Quantifying the Early Immune Response and Adaptive Immune Response Kinetics in Mice Infected with Influenza A Virus. *J Virol* 84:6687–6698
- Murali-Krishna K, Altman J, MSuresh, Sourdive D, Zajack A, Miller J, Slansky J, Ahmed R (1998) Counting Antigen-Specific CD8 T Cells: a Reevaluation of Bystander Activation during Viral Infection. *Immunity* 8:177–187
- Nordon R, Nakamura M, Ramirez C, Odell R (1999) Analysis of growth kinetics by division tracking. *Immunol and cell biol* 77:523–529
- Oseroff C, Peters B, Pasquetto V, Moutaftsi M, Sidney J, Panchanathan V, Tschärke D, Maillere B, Grey H, Sette A (2008) Dissociation between epitope hierarchy and immunoprevalence in CD8 responses to vaccinia virus western reserve. *J Immunol* 180:7193–7202
- Pamer E (2004) Immune responses to *Listeria monocytogenes*. *Nature Reviews Immunology* 4:812–823
- Parker R, Bronson L, Green R (1941) Further studies of the infectious unit of vaccinia. *The Journal of experimental medicine* 74:263–281

- Rehm K, Connor R, Jones G, Yimbu K, Mannie M, Roper R (2009) Vaccinia virus decreases major histocompatibility complex (MHC) class II antigen presentation, T-cell priming, and peptide association with MHC class II. *Immunology* 128:381–392
- Rouzine I, Murali-Krishna K, Ahmed R (2005) Generals die in friendly fire, or modeling immune response to HIV. *J Computational and Appl Math* 184:258–274
- Saenz R, Quinlivan M, Elton D, MacRae S, Blunden A, Mumford J, Daly J, Digard P, Cullinane A, Grenfell B, McCauley J, Wood J, Gog J (2010) Dynamics of Influenza Virus Infection and Pathology. *J Virol* 84:3974–3983
- Snyder J, Belyakov I, Dzutsev A, Lemonnier F, Berzofsky J (2004) Protection against Lethal Vaccinia Virus Challenge in HLA-A2 Transgenic Mice by Immunization with a Single CD8 T-Cell Peptide Epitope of Vaccinia and Variola Viruses. *J Virol* 180:7052–7060
- Su M, Wlادن P, Golan D, Eisen H (1993) Cognate peptide-induced destruction of CD8⁺ cytotoxic T lymphocytes is due to fratricide. *J Immunol* 151:658–667
- Sun S, Zhao G, Xiao W, Hu J, Guo Y, Yu H, Wu X, Tan Y, Zhou Y (2011) Age-related sensitivity and pathological differences in infections by 2009 pandemic influenza A (H1N1) virus. *J Virol* 8:52
- Terry E, Marvel J, Arpin C, Gandrillon O, Crauste F (2012) Mathematical Model of the primary CD8 T Cell Immune Response: Stability Analysis of a Nonlinear Age-Structured System. *J Math Bio*
- Tridane A, Kuang Y (2010) Modeling the interaction of cytotoxic T lymphocytes and influenza virus infected epithelial cells. *Math Biosci Eng* 7:171–185
- Wolk K, Lazarowski E, Traylor Z, Erin N, Jewell N, Durbin R, Durbin J, Davis I (2008) Influenza A virus inhibits alveolar fluid clearance in BALB/c mice. *American journal of respiratory and critical care medicine* 178:969–976
- Wong P, Pamer E (2003) CD8 T cell responses to infectious pathogens. *Annual review of immunology* 21:29–70

Table 4: Percentage of frequency of tested parameter values, in the 0.01% of parameter sets corresponding to the smallest errors (and so to the best fits). Each bar in histograms corresponds to a percentage of appearance of a parameter value (see in the first column for these values, associated to the bars by colors). The sum of the 5 values of each histogram always equals 100%.

Parameters	Influenza virus experiment	Vaccinia virus experiment	Listeria bacteria experiment
ρ_E (Day ⁻¹) ■ 10 ^{^-1} ■ 5.10 ^{^-1} ■ 1 ■ 5 ■ 10			
μ_P (Cell ⁻¹ Day ⁻¹) ■ 10 ^{^-8} ■ 10 ^{^-7} ■ 10 ^{^-6} ■ 10 ^{^-5} ■ 10 ^{^-4}			
δ_{NE} (Day ⁻¹) ■ 10 ^{^-2} ■ 5.10 ^{^-2} ■ 10 ^{^-1} ■ 5.10 ^{^-1} ■ 1			
μ_P^0 (Day ⁻¹) ■ 10 ^{^-3} ■ 10 ^{^-2} ■ 10 ^{^-1} ■ 1 ■ 10			
ρ_P (Day ⁻¹) ■ 10 ^{^-3} ■ 10 ^{^-2} ■ 10 ^{^-1} ■ 1 ■ 10			
μ_E (Cell ⁻¹ Day ⁻¹) ■ 10 ^{^-8} ■ 5.10 ^{^-8} ■ 10 ^{^-7} ■ 5.10 ^{^-7} ■ 10 ^{^-6}			
μ_N (Day ⁻¹) ■ 10 ^{^-4} ■ 10 ^{^-3} ■ 10 ^{^-2} ■ 10 ^{^-1} ■ 1			
δ_{EM} (Day ⁻¹) ■ 10 ^{^-3} ■ 10 ^{^-2} ■ 10 ^{^-1} ■ 1 ■ 10			
μ_M (Day ⁻¹) ■ 5.10 ^{^-2} ■ 10 ^{^-1} ■ 5.10 ^{^-1} ■ 1 ■ 5			